

Adaptive Guidance Systems for Hypersonic Reusable Launch Vehicles¹

John D. Schierman, David G. Ward, Jason R. Hull, Jeffrey F. Monaco
Barron Associates, Inc.
1160 Pepsi Place, Suite 300
Charlottesville, VA 22901
804-973-1215
lastname@barron-associates.com

Michael J. Ruth
Orbital Sciences Corp.
21700 Atlantic Blvd.
Dulles, VA 20166
703-406-5785
Ruth.Michael@orbital.com

Abstract— This paper presents an adaptive guidance system approach applied to hypersonic Reusable Launch Vehicles (RLVs). After an effector failure, it is assumed that the inner-closed-loop system utilizes a reconfigurable control algorithm to recover nominal maneuvering capabilities to the extent possible. However, nominal performance will typically not be fully recovered for RLVs, and the outer-loop guidance system must account for the degraded vehicle response. Two main approaches for the adaptive guidance system are presented. The first approach augments the existing production guidance system by adding adaptation capabilities. A case study shows that stability is maintained following a primary pitch effector failure. This is achieved by adapting gains in the guidance feedback loops. However, it is shown that the trajectory commands to the guidance loops must also be re-targeted in order to achieve a safe landing. The second approach employs an on-line optimal trajectory re-targeting algorithm. Here, the calculus of variations is used to generate a database of admissible neighboring extremals. This database is then encoded in an efficient manner to generate mappings between the current states and vehicle capabilities and the costates defining the admissible optimal trajectories. These mappings are interrogated on-line at regular intervals to obtain the optimal guidance commands. A proof-of-concept case study of this approach shows that the final landing conditions are achieved following a primary speed control effector failure.

TABLE OF CONTENTS

1. INTRODUCTION
2. DEMONSTRATION PLATFORM
3. THE OVERALL GUIDANCE APPROACH
4. ADAPTIVE PRODUCTION GUIDANCE (APG) APPROACH
5. CASE STUDY: APG APPROACH
6. OPTIMUM-PATH-TO-GO/ADAPTIVE PRODUCTION GUIDANCE (OPTG/APG) APPROACH
7. ADVANCED OPTG APPROACH
8. CASE STUDY: ADVANCED OPTG APPROACH
9. CONCLUSIONS

1. INTRODUCTION

Both NASA and the Air Force have recently expressed interest in developing technologies that will increase the reliability and safety of launch vehicles to near commercial fleet levels. Both organizations have recognized that on-board reconfiguration capabilities will be *essential* to achieve these goals. Hypersonic Reusable Launch Vehicles (RLVs) must operate over a very wide flight envelope (Mach 0-25, Altitude 0-500+Kft), and vehicle attitude and flight path must be tightly controlled throughout this envelope to ensure that the airframe remains within a number of different constraints (thermal, structural, stability, etc). In some cases (e.g., re-entry or auto-landing), the "corridor" of allowable trajectory responses is quite narrow. Further, there are unique challenges in determining the

¹ 0-7803-6599-2/01/\$10.00 © 2001 IEEE.

dynamics of these vehicles compared to other fixed-wing aircraft. Two key difficulties are that high-Mach wind tunnel tests are less representative of the actual aircraft dynamics, and at hypersonic velocities, accurate measurements can be difficult to obtain, thus parameter identification from flight data is more challenging than with conventional aircraft. Added to this uncertainty is the possibility that failure of a critical control component (e.g., elevon effector) might drive the vehicle to near or beyond its allowable guidance corridor limits. If the control and guidance systems are not quickly reconfigured, recovery of the vehicle might not be possible.

Meanwhile, RLV designs are influenced by weight and other constraints that rarely allow for significant effector redundancy to *completely* recover the pre-failure closed-loop dynamics using inner-loop reconfiguration strategies alone. Therefore, it is likely that even after inner-loop reconfiguration the closed-loop dynamics will change. This leads to the desire to investigate adaptive autonomous control *and* guidance systems that reconfigure for unforeseen dynamics in the inner-loop to the extent possible and then *recompute* realizable guidance trajectories and autopilot commands based on the new inner-loop dynamics and possibly evolving mission objectives.

The focus of this paper is on the development of an adaptive guidance system that would ultimately work in conjunction with an inner-loop reconfigurable control system.

2. DEMONSTRATION PLATFORM

The demonstration platform used in the developments presented herein was Orbital Science Corporation's X-34 hypersonic rocket plane, shown in Figure 1 [1-2]. It is a reusable, suborbital, air-launched vehicle designed to operate in a broad hypersonic flight envelope of speeds approaching Mach 8 at altitudes up to 50 miles. It will be air-launched from Orbital's L-1011 Tri-Star carrier aircraft currently used to launch the Pegasus expendable launch vehicle. The vehicle weighs approximately 17,000 lb. and is powered by the Fastrac single-stage engine that burns a mixture of liquid oxygen and kerosene. Its length, wingspan, and release weight are roughly equal to the current Pegasus XL launch vehicle.

The program plans to complete production of three X-34 vehicles. It is expected that the final vehicle will be used in a series of powered flight tests beginning in approximately the year 2002. One of the main objectives of the X-34 program is to develop and demonstrate advanced technologies that will benefit future hypersonic RLV production systems.

The focus of the guidance system development herein is on the longitudinal motion of the vehicle during the approach-to-landing phase of flight. Its primary control effectors in

this phase are elevons to control pitching motion, speedbrake to adjust velocity due to head/tail winds and reject gust disturbances, and body flap for additional pitch trim control.



Figure 1. Orbital Sciences Corp. X-34 Hypersonic Reusable Launch Vehicle.

3. THE OVERALL GUIDANCE APPROACH

The high level architecture of the guidance and control systems are shown in Figure 2. There are two main aspects to this approach.

1. The outer-loop performs its own identification of inner-closed-loop dynamics and guidance law reconfiguration acts *independent* of the inner-loop reconfiguration.
2. The guidance system incorporates a long-horizon on-line trajectory re-targeting algorithm which drives a primary adaptable guidance system. The primary guidance system is tasked to maintain flight stability - critical during the recovery stage from an effector failure or sudden change in the system's dynamics. The primary guidance system is updated sufficiently fast enough to run in real time. In contrast, the trajectory re-targeting algorithm is expected to be computationally more intensive, and will run in *near* real-time, at a slower update rate.

The authors believe this *modular* approach allows for more freedom in the development/implementation of such a system. The design engineers can choose between several options for inner-loop control reconfiguration, primary guidance adaptation and trajectory re-targeting schemes to best fit the needs of the particular application.

Two main guidance system approaches have been developed and are discussed next.

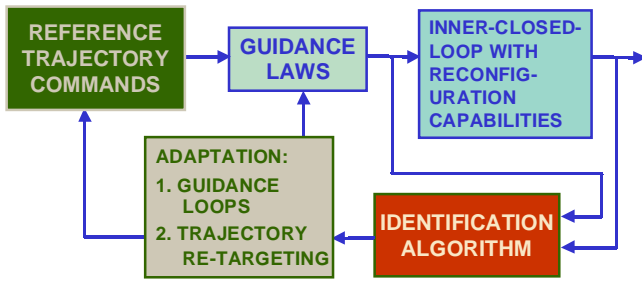


Figure 2. High Level Architecture for Reconfigurable Control/Guidance System.

4. ADAPTIVE PRODUCTION GUIDANCE (APG)

APPROACH

Our approach here is to integrate reconfiguration capabilities into the current production guidance system. We define this as the Adaptive Production Guidance (APG) formulation. The purpose of this work is to offer a lower-risk, nearer-term solution to maintain flight stability and improve performance under effector failures or significant aerodynamic modeling errors.

A simplified presentation of the altitude (H) guidance loops for this approach is given in Figure 3. Here, the primary guidance module includes a gain adaptation algorithm that varies the feedback gains on altitude and altitude rate errors, depending on the current estimate of inner-loop capabilities. The figure indicates that the Modified Sequential Least Squares (MSLS) parameter identification algorithm [3] provides information regarding the current capabilities of the inner-closed-loop system to the adaptation algorithm. It will be shown that this method provides rapid gain adaptation to maintain stability immediately following a severe elevon failure which significantly reduces the inner-loop bandwidth.

Figure 3 also shows reconfiguration of the reference command signals. Here, the parameter identification algorithm provides information to a reference altitude and altitude rate command adaptation algorithm. It is shown that reconfiguration of these reference command signals is necessary to safely land the vehicle. A simplified re-targeting scheme was investigated for the case study, discussed next.

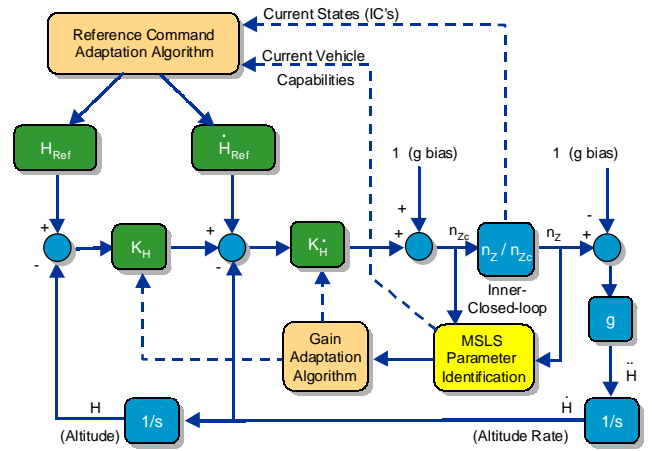


Figure 3. Altitude Guidance Loops for Adaptive Production Guidance (APG) System.

5. CASE STUDY: APG APPROACH

In this section we present results of the Adaptive Production Guidance (APG) methodology. A preliminary study of the approach-to-landing problem under elevon failures is presented. Again, the demonstration platform is Orbital Science Corporation's X-34 hypersonic RLV. Altitude, velocity, and flight path profiles specific to the X-34's approach-to-landing trajectory have been provided by Orbital and integrated into the study. Further, the altitude and altitude rate guidance loop architectures used in this study closely approximate the production guidance system currently in use in the X-34 program.

The inner-closed-loop vehicle is represented by the transfer function from normal acceleration to its respective command, or n_z/n_{zc} . Here,

$$\frac{n_z(s)}{n_{zc}(s)} = \left(\frac{-\omega_n^2}{z^2} \right) \frac{(s+z)(s-z)}{s^2 + 2\zeta\omega_n s + \omega_n^2} \quad (1)$$

where,

$$\begin{aligned} z &= 2 \text{ rad/sec (zero location)} \\ \zeta &= 0.6 \text{ (inner-closed-loop damping)} \end{aligned} \quad (2)$$

Nominal System Results

For the nominal system, the inner-closed-loop natural frequency was:

$$\omega_n = 1.6 \text{ rad/sec} \quad (3)$$

The feedback gains were chosen to be:

$$K_H = 0.39 \quad \& \quad K_{\dot{H}} = 0.022 \quad (4)$$

These values can be shown to give at least 6 dB of gain margin and over 45 degrees of phase margin for each loop.

Figure 4 presents a close up of the nominal vehicle's approach-to-landing trajectory near landing, starting from an altitude of 10,000 ft. Trajectory integration actually began at an altitude of 30,000 ft. Note that altitude plotted is altitude above the runway, not above sea level. Both the altitude reference command (H_{Ref}) and the altitude response (H) are plotted. It is evident that the vehicle follows the reference command quite accurately. The trajectory begins at a steep glideslope with a flight path angle = -17 deg. Here, it can be seen that after the first flare, the glideslope becomes quite shallow, and the flight path angle rapidly reduces from -2 degrees to near zero degrees at landing. Although not simulated, a final flare maneuver would be executed just before landing to make final adjustments to the terminal velocity and arrest the touchdown sink rate.

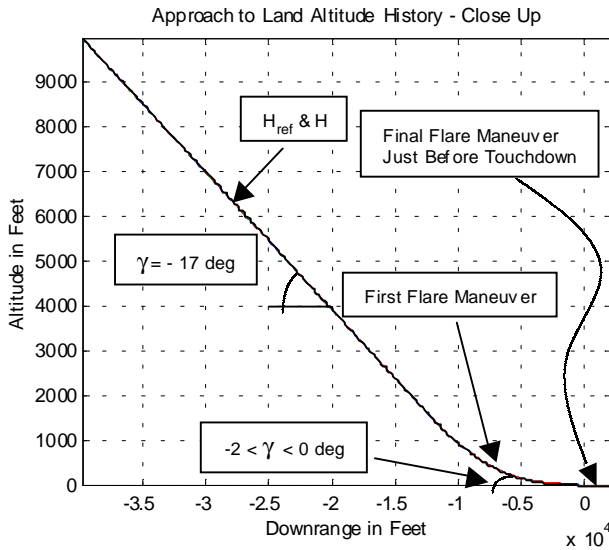


Figure 4. Nominal Vehicle's Approach-to-Landing Trajectory.

Figure 5 presents the sink rate time history for the nominal vehicle. Again, the vehicle's response closely follows the reference command signal. The sink rate approaches near zero at touchdown. The performance of the nominal design is considered to be excellent.

Failed Elevon/No Guidance Reconfiguration Results

We now consider an elevon failure. We assume that an inner-loop control reconfiguration will properly adapt to a failed elevon by controlling pitch attitude dynamics with the only other available pitch control effectors, body flap and speed brake. However, nominal performance can never be recovered in this case because the bandwidths of the body flap and speed brake are much slower than that of the elevon effector. Under an elevon failure, inner-loop reconfiguration is expected to reduce the natural frequency in the normal acceleration transfer function (see Eq. (1)) to approximately:

$$\omega_n = 0.4 \text{ rad/sec} \quad (5)$$

The elevon failure was modeled to occur at 80 seconds into the flight (approximately 10,000 ft in altitude) by appropriately reducing ω_n to the value given in Eq. (5) at that time.

Figure 6 presents the approach-to-landing trajectory for this case when no outer-loop guidance reconfiguration was mechanized. The altitude and altitude rate loop gains were held constant at their nominal values. It can be seen in the figure that without guidance reconfiguration, the vehicle's trajectory goes unstable, resulting in loss of the vehicle.

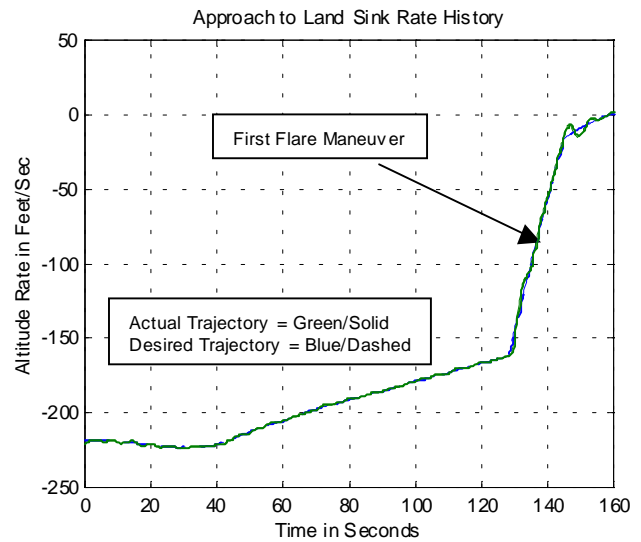


Figure 5. Nominal Vehicle's Sink Rate Time History.

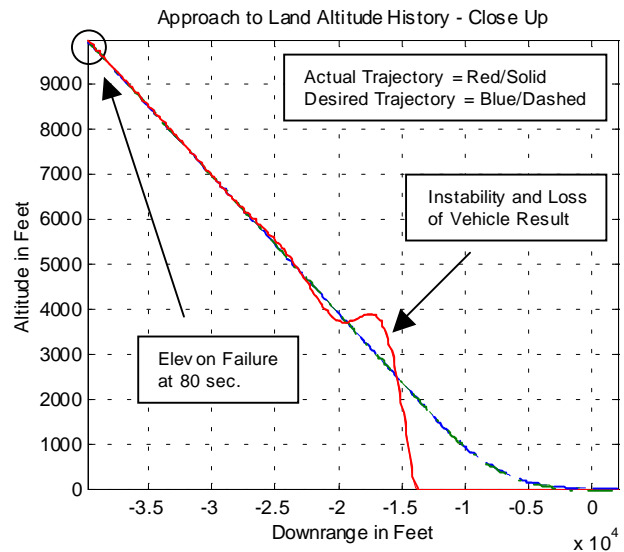


Figure 6. Approach-to-Land Trajectory Under Elevon Failure - With No Guidance Reconfiguration.

Failed Elevon With Guidance Reconfiguration

We next integrated a primary guidance reconfiguration scheme into the system. This included a Modified Sequential Least Squares (MSLS) algorithm [3] coupled with a guidance gain adaptation law (see Figure 3). In a sequential loop closure fashion, several loop gain values for the altitude and altitude rate loops were designed as the inner-loop bandwidth was ranged from its nominal value to the value under speed brake/body flap reconfiguration. The gain values were designed to achieve gain margins between 6 and 7 dB and phase margins not less than 45 degrees. For computational efficiency, the gain adaptation algorithm was defined as curve fits to the design data. The gain adaptation laws were:

$$\begin{aligned} K_H &= -1.3510e-001 \Omega + 7.1888e-002 \\ K_{\dot{H}} &= -2.5736e-003 \Omega^3 - 1.2776e-002 \Omega^2 \\ &\quad - 2.3127e-002 \Omega + 3.3534e-003 \end{aligned} \quad (6)$$

where $\Omega = -\omega_n^2$, and ω_n is the inner-closed-loop bandwidth (see Eq. (1)). These functions were defined in this manner because the MSLS algorithm directly identifies the parameter Ω .

Figure 7 plots the adaptation laws given by Eq. (6), and the corresponding design data. It was determined by simulation that the accuracies of the curve fits were adequate.

Next, we turn our attention to the MSLS identification results. To model the real world effects of measurement noise, subsequent filtering and state reconstruction, filtered noise was added to the outputs of the inner-closed-loop model. Figure 8 presents the inner-loop bandwidth parameter, Ω , and its MSLS estimate. Note that identification of the new value at 80 seconds is almost immediate. The reason for such rapid identification is that at the time of failure there is a substantial change in the inner-closed-loop responses, which, due to feedback, excites the commanded acceleration into the inner-closed-loop system (not shown). Because of this rapid excitation, the new values for the model parameters are quickly identified. In reality, since the inner-loop control system may take time to reconfigure to the slower control effectors, identification of the new bandwidth may not be as rapid as shown here. However, as shown in Figure 6, the vehicle travels for approximately 17,000 ft (or, approximately, 25 seconds) before significantly departing from the nominal trajectory. Real world effects such as wind gusts will most likely cause the instability to appear sooner than in this case, but based on past experience, the benign flight characteristics of an RLV's entry/approach should allow for more than enough time for both the inner and outer-loop identification and reconfiguration procedures to stabilize the system.

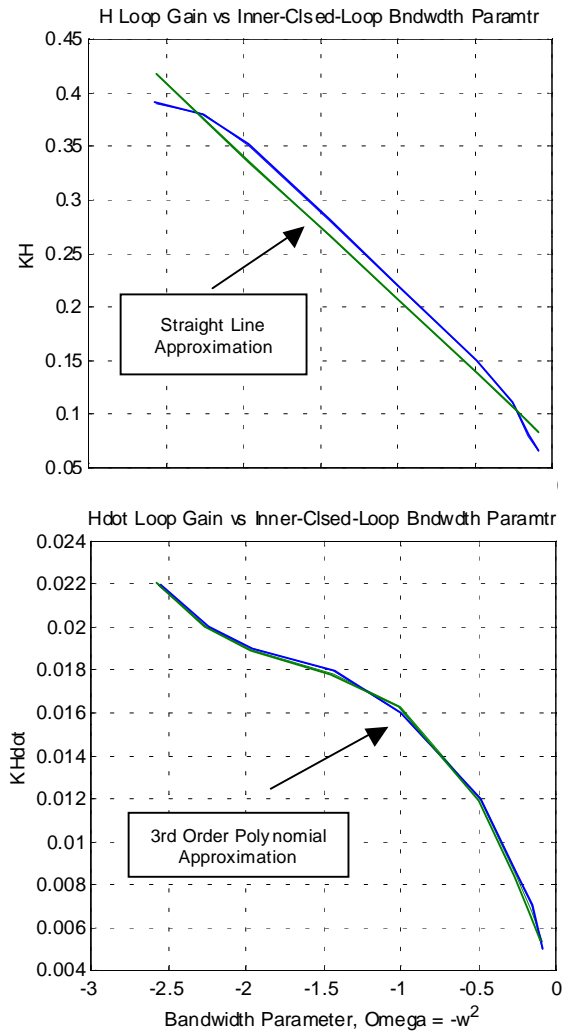


Figure 7. Altitude/Altitude Rate Loop Gains –vs- Ω For Acceptable Gain and Phase Margins.

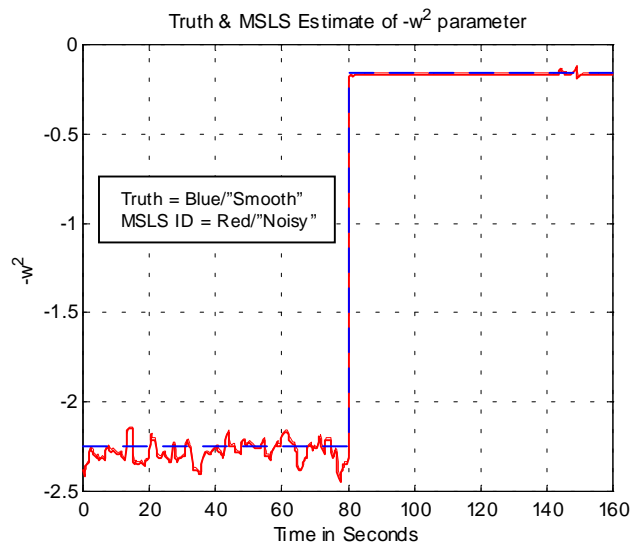


Figure 8. MSLS Estimate of Inner-Closed-Loop Bandwidth Parameter, Ω .

Figure 9 presents the altitude and altitude rate loop gain time histories. Because of the rapid identification of the change in the inner-loop bandwidth, these gains also rapidly change to their new values corresponding to adaptation laws given in Eq. (6). Note that the time histories seen in both Figure 8 and Figure 9 are more irregular before the elevon failure and smoother afterwards. Again, this is due low excitation of the system preceding the failure and increased control activity following the failure.

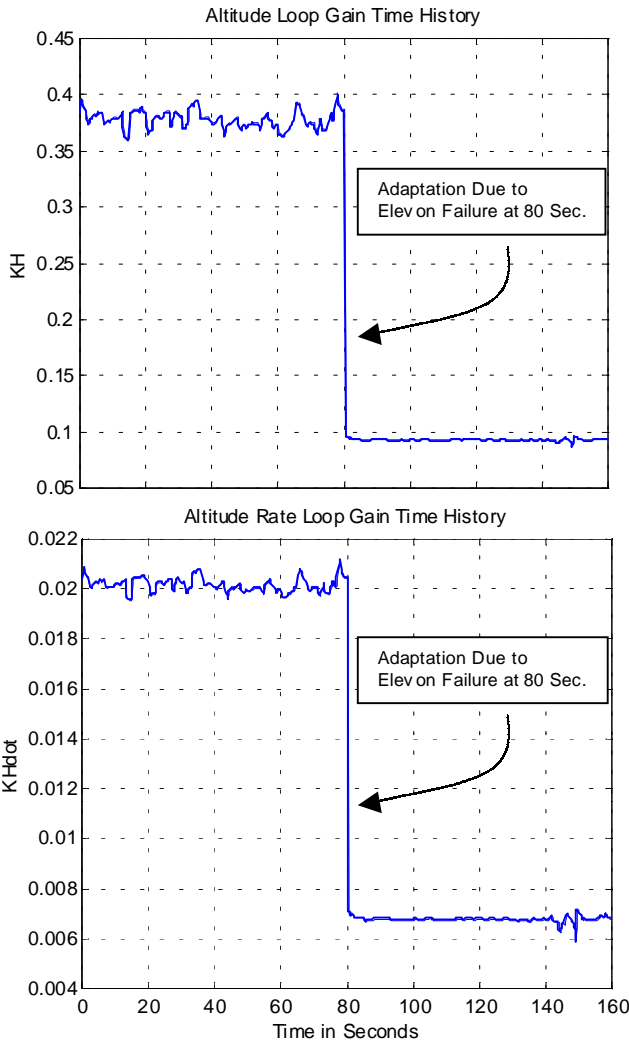


Figure 9. Altitude and Altitude Rate Loop Gain Time Histories.

Figure 10 presents the trajectory for the case of failed elevator with guidance gain adaptation. It can be seen that stability is maintained following the failure at 80 seconds. However, because of the reduced maneuvering capabilities of the vehicle, it can no longer follow the first flare, then overcorrects and lands at a sink rate of -20 ft/sec, (flight path angle of -4 degrees). This would most likely cause severe damage to the vehicle. Methods to remedy this situation are discussed next.

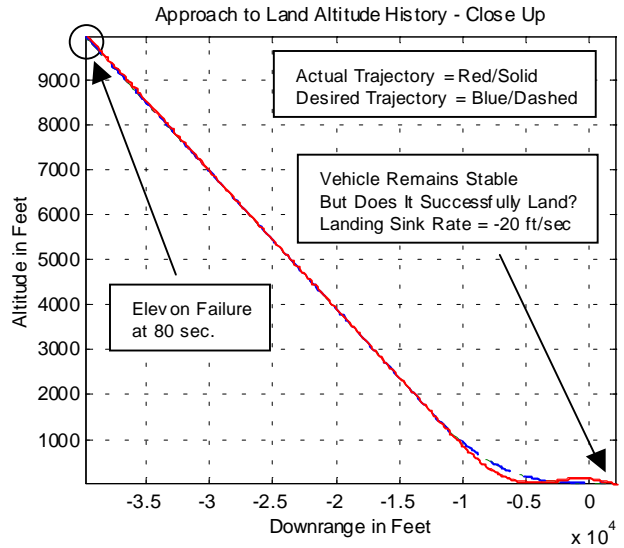


Figure 10. Approach-to-Land Trajectory Under Elevon Failure - With Guidance Reconfiguration.

Several preliminary re-targeted trajectories were studied to investigate trajectory/guidance loop interaction. Here, new trajectories were designed to abate the required commanded accelerations; hence, the radius of curvature for the flares of each candidate trajectory was increased from the nominal reference trajectory. Further, note that the re-targeted trajectories were designed beginning from the point of failure. Unfortunately, little improvement was seen in the landing conditions. The best sink rate obtained with re-targeting was -18 ft/sec, only a small reduction over no re-targeting (see Figure 10). This study indicates the following:

1. Even if one is afforded the luxury of knowing when the failure occurs, and designs alternative trajectories from that point, it is a difficult task to manually find a solution which achieves desired touchdown conditions by making simple modifications to the baseline trajectory (ex. reducing the maximum acceleration).
2. If such a scheme were to be implemented, then to cover effector failures throughout the trajectory would require designing re-targeted trajectories at regular intervals throughout the mission segment. Here, the “curse of dimensionality” rules out this approach. It would be a formidable challenge to *manually* design enough re-targeted trajectories such that a viable solution can be found on-line at any time during the mission after an effector failure.
3. The difficulties seen in this case study indicate that the re-targeted trajectory must account for the reduced maneuvering capabilities, be designed to achieve all the final touchdown conditions (ex. sink rate, velocity, etc.), be stored in an efficient manner on-line, and be generated in some automated manner. This leads us to the approach discussed in the next section.

6. OPTIMUM-PATH-TO-GO/ADAPTIVE PRODUCTION GUIDANCE (OPTG/APG) APPROACH

Optimization techniques have been widely studied for hypersonic vehicle trajectory designs [4-10]. Here, the Optimal-Path-To-Go (OPTG) [11-12] algorithm is utilized to generate new reference altitude and altitude rate commands *on-line*. These new commands are designed to be optimal (or near optimal) with the production guidance law structure (feedback loops on altitude and altitude rate), and the adaptive guidance gains (i.e. the APG system discussed previously). Figure 11 presents the block-diagram of this approach, now termed the OPTG/APG system. Structurally, the feedback loops remain the same as in the APG approach (Figure 3). The only difference is that now the reference commands are generated on-line via the OPTG method.

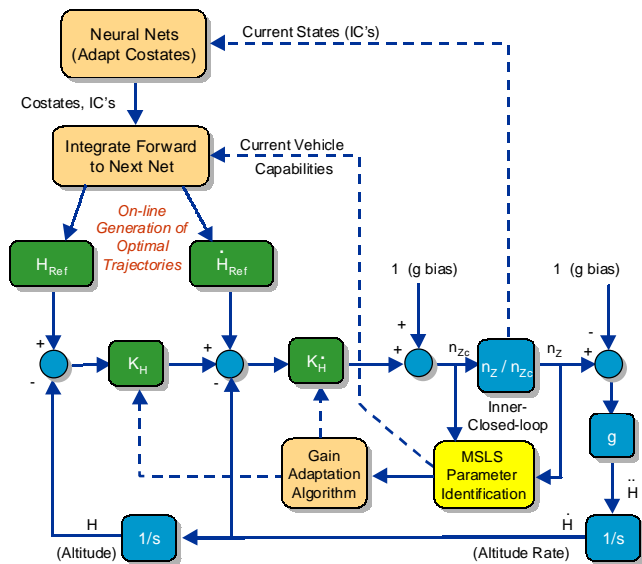


Figure 11. On-Line Generation of Optimal Trajectories in the OPTG/APG System.

The OPTG methodology consists of the following three main elements:

1. **Off-Line Trajectory Generation:** Form sets of numerous representative optimal trajectories which are valid for the current mission and vehicle capabilities. Here, the Calculus of Variations (COV) [13-14] approach is used to formulate the optimization problem.
2. **Off-Line Trajectory Encoding:** From the set of neighboring optimal extremals found in Step 1, one has a single set of state-costate pairs that define any given optimal trajectory. Polynomial neural networks can then be employed to learn mappings between the *observable* vehicle states and the costates at different points in the flight space. Not only do the networks provide an efficient, compact “table lookup” that

parameterizes the costates as functions of current vehicle *observables* (states and capabilities), but they provide for interpolation between extremals so that on-line, one need not command the vehicle to go to a neighboring extremal, but can instead generate nearly instantly an approximate extremal trajectory from the current point to the touchdown point.

3. **On-Line Trajectory Integration** – The final step in the OPTG approach is performed on-line. Trajectories are reshaped in flight to account for changes in the vehicle dynamics. During flight, the current vehicle states are used to compute an appropriate set of costates from the on-board neural network mappings of Step 2. With these states and co-states as starting values, the vehicle dynamics and costate equations are integrated forward for a specified duration and used to compute the new reference trajectories. The loop is closed by re-initializing the costates at regular intervals – typically on the order of 1 Hz. Figure 12 illustrates the parameter space of admissible starting points along the trajectory, and the on-line trajectory reshaping strategy. Note that only two dimensions (altitude and downrange) are illustrated in the figure for clarity. However, for the present formulation, the inputs to the neural networks would include the current altitude, downrange, flight path angle, velocity, identified inner-loop bandwidth and identified drag coefficient. These last two parameters define the current vehicle capabilities and enable on-line trajectory reconfiguration. From our studies to date, we believe that the outer-loop identification algorithm need only identify a small number of critical parameters, such as inner-closed-loop bandwidth, the total drag on the vehicle, or C_{L-max} , or the lift-to-drag ratio to convey the vehicle’s “current health” to the PNN model. (It is the job of the inner-loop identification algorithm to identify specific control effector failures and other model details required for *control* reconfiguration.)

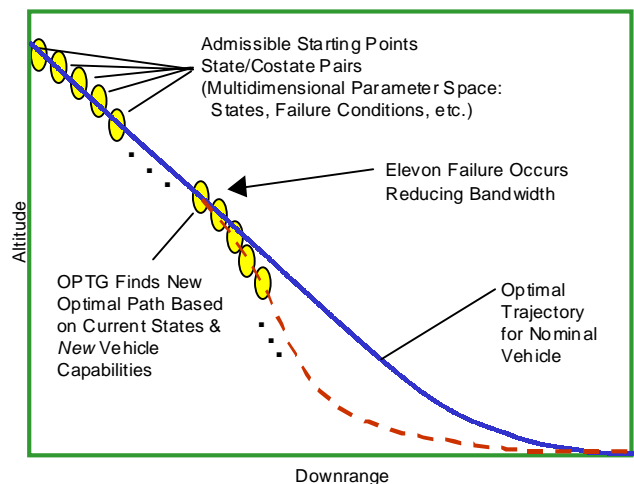


Figure 12. OPTG Trajectory Reshaping Strategy.

This method gives us a solution to the problem found in the case study. Here, entire extremal trajectories can be represented by a single vector of costate variables (or Lagrange multipliers). Then, the pre-trained neural networks can be used to store these costate variables as a function of current vehicle capabilities and states. This provides an efficient way of storing admissible trajectories that start at *any* point in the flight envelope.

Integration of the OPTG algorithm into the APG system is underway at the time of this writing. Case study results are expected to be released in future publications. A related OPTG approach is presented next.

7. ADVANCED OPTG APPROACH

Figure 13 presents an alternative to the OPTG/APG system architecture shown in Figure 11. For the OPTG/APG formulation, the model of the system consists of the adaptive altitude and altitude rate loops *wrapped around the inner-closed-loop vehicle*. The commands generated are reference altitude and altitude rate trajectories. In that formulation, the APG system generates the guidance commands into the inner-closed-loop system. In contrast, Figure 13 shows that the OPTG strategy is used to *directly generate the guidance commands into the inner-closed-loop system*. The production guidance law approach is discarded. Here, the model of the system used in the OPTG algorithm consists only of the inner-closed-loop vehicle (not the altitude/rate loops). This is considered a more advanced, longer-term approach that offers more flexibility in the guidance reconfiguration. This approach is termed the Advanced OPTG formulation.

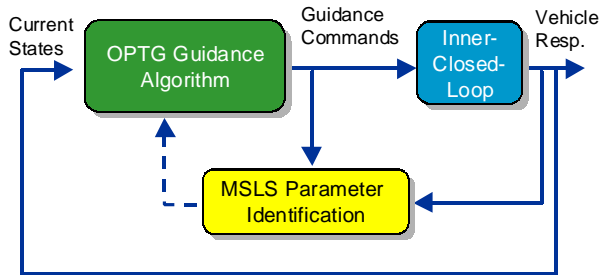


Figure 13. Advanced OPTG Guidance Architecture – Direct Generation of Guidance Commands To the Inner-Closed-Loop System.

8. CASE STUDY: ADVANCED OPTG APPROACH

We began our development of the Advanced OPTG approach by generating optimal trajectories for the X-34 during the approach-to-landing phase of flight. The problem was set up such that for the on-line trajectory generation algorithm, an optimal angle of attack command was generated, which was fed directly to the inner-closed-loop

system. For this preliminary study, the body flap and speed brake were assumed fixed at their nominal trim values of -5° and 60° , respectively. Inclusion of a velocity command to be optimized (ultimately involving the speed brake) will be investigated in future work. This should benefit the vehicle's overall performance during a nominal approach trajectory.

In developing the calculus of variations (COV) to generate optimal trajectories, the case of speed brake failures was investigated. At mid-course in the trajectory, the speed brake was modeled to go from its nominal setting of 60° to its maximum setting of 90° .

The governing equations of motion that were used in the COV derivation are presented next. The conventional “flight path” model governs the velocity and flight path motion, and an approximation to the higher fidelity X-34 aerodynamic force model, provided by Orbital, was used. Figure 14 presents the free-body diagram of the X-34 for longitudinal motion.

The states of the system are considered to be:

1. V = vehicle velocity ~ ft/sec
2. γ = flight path angle ~ radians
3. X = downrange position ~ feet
4. H = altitude ~ feet

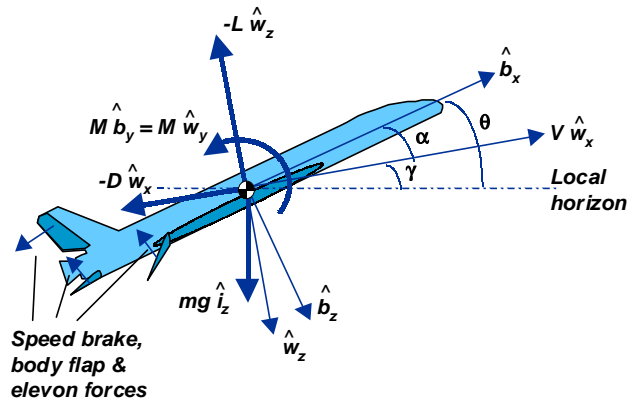


Figure 14. Free-Body Diagram of the X-34 Vehicle Under Longitudinal Motion.

It can be shown that the governing equations of motion and kinematic relations for this system are:

$$\begin{aligned} \dot{V} &= \left(\frac{-D}{m} - g \sin(\gamma) \right) t_f \\ \dot{\gamma} &= \left(\frac{L}{mV} - \frac{g}{V} \cos(\gamma) \right) t_f \\ \dot{X} &= (V \cos(\gamma)) t_f \\ \dot{H} &= (V \sin(\gamma)) t_f \end{aligned} \quad (8a)$$

where,

$$\begin{aligned}
L &= \bar{q}S C_L(\alpha, \delta_{sb}, \delta_{bf}) \\
D &= \bar{q}SC_D(\alpha, \delta_{sb}, \delta_{bf}) \\
\bar{q} &= \frac{1}{2}\rho(H) \mathcal{V}^2
\end{aligned}
\tag{8b}$$

Additional governing equations required for the COV formulation are:

$$\begin{aligned}
\dot{H}_{lim} &= \left[(H - \hat{H})^2 U(\hat{H} - H) \right]_{t_f} \\
\dot{t}_f &= 0
\end{aligned}
\tag{9}$$

Here, t_f represents a “final time” state and is included in the formulation because this is a free final time problem. This state multiplies the time step and acts to adjust the total integration time. This allows the COV approach to solve for an optimal length of time for completion of the trajectory. In the equation governing the state H_{lim} , \hat{H} is the ground altitude and U is the unit step function. The function defining \dot{H}_{lim} can never take on negative values, and takes on positive values if the vehicle ever drops below the ground altitude. The state H_{lim} was then constrained to be zero at the initial and final times. In order to meet these boundary conditions, this forces the solution to never allow the vehicle to fall below the ground altitude (\dot{H}_{lim} must remain zero for all time).

Note that lift and drag $\{L, D\}$ in the above equations are total aerodynamic forces and moments due to non-zero angle of attack and all control surface deflections. To mimic an inner-closed-loop vehicle without specifically accounting for the rotational dynamics in the optimization, the coefficients of lift and drag can be approximated by the following formulas:

$$\begin{aligned}
C_L &= 0.05\alpha - 0.0014 \\
C_D &= 8.9 \times 10^{-5} \alpha^2 - 4.8 \times 10^{-3} \alpha + 2.2 \times 10^{-6} sb^2 \\
&\quad + 2.5 \times 10^{-4} sb + 1.7 \times 10^{-2}
\end{aligned}
\tag{10}$$

These formulas were derived by curve fitting a high fidelity model of the X-34 aerodynamics whereby the elevon deflection was solved at each angle of attack to trim the vehicle in pitch. Varying the speed brake angle will move the C_D curve along the vertical axis. This was done to model the speed brake failure. Other nonlinear effects, such as dropping the landing gear, were also included in the drag model. The angle of attack command was limited to within $\pm 10^\circ$ to stay within the region where the approximate aerodynamic model is most accurate.

Finally note that the air density model, $\rho(H)$, in Eq. (8b) was derived from a Vandenburg AFB atmosphere model supplied by Orbital.

The cost function to be minimized was defined to be:

$$\begin{aligned}
J &= \frac{1}{2} K_1 (\mathcal{V}_{t_f} - \hat{\mathcal{V}}_{t_f})^2 \\
&\quad + \frac{1}{2} \int_{t_i}^{t_f} \{ K_2 (\alpha - \alpha_{ref})^2 + K_3 (\alpha - \alpha_{prev})^2 \} dt
\end{aligned}
\tag{11}$$

The first term in this cost function minimizes the difference between the final velocity and the specified desired value, $\hat{\mathcal{V}}_{t_f}$. The first term in the integrand minimizes the angle of attack control effort from a desired profile α_{ref} (note, α_{ref} was derived from nominal trajectories supplied by Orbital), while the second term in the integrand minimizes the difference between the current angle of attack command and the previous command value. This term keeps the command rates within reasonable values. Note, the first and second terms in the integrand are not independent, and can be combined where the objectives are “ranked” by the relative weightings, K_2 and K_3 .

The initial and final conditions were defined as follows:

$$\begin{aligned}
V_{t_i} &= 633 \text{ ft/s} & V_{t_f} &= 328 \text{ ft/s} \\
\gamma_{t_i} &= -17^\circ & \gamma_{t_f} &= 0^\circ \\
X_{t_i} &= -109,160 \text{ ft} & X_{t_f} &= 2,150 \text{ ft} \\
H_{t_i} &= 35,030 \text{ ft} & H_{t_f} &= 3,838 \text{ ft}
\end{aligned}
\tag{12}$$

The initial conditions represent typical values for the X-34 at approximately 30,000 ft above the runway, and 20 nautical miles downrange. Note here that the runway altitude is 3,828 feet above sea level. (Hence the value for the final altitude.) The final downrange position represents the end of the runway. Using a final flight path angle of 0° will ensure a minimal sink rate.

For this proof-of-concept study, two sets of neighboring extremals were generated. One set at the beginning of the trajectory corresponding to the nominal vehicle, and the other set near the point of speed brake failure, corresponding to the vehicle with this failure (increased drag). Figure 15 shows these sets of optimal trajectories. Note that the shooting method [13] was used to obtain optimal trajectory solutions, and relatively little time is needed to generate large sets of neighboring extremals. The engineering challenge comes in finding the *first* valid solution. Two polynomial neural networks were then encoded corresponding to the two sets of trajectories shown in Figure 15, with downrange and altitude as the inputs, and valid co-states as the outputs. For the case study, the first

network was interrogated at the beginning of the simulation, and the second was interrogated at the time of failure.

Figure 16 shows that without reconfiguration, the vehicle is lost, hitting the ground far short of the runway. The added drag due to the speed brake failing wide open causes a significant reduction in the vehicle's energy-to-downrange ratio. With the OPTG guidance system, the vehicle's flight path is immediately turned up after the speed brake failure to extend the range under the added drag. Note the sharp jump in angle of attack at this point in Figure 17. This figure also shows that the final touchdown conditions are nearly all met. The final sink rate is less than 7 ft/sec, and the final velocity is actually less than the required final velocity. Note that for the reconfigured trajectory, the vehicle stays aloft approximately 20 seconds longer than for the nominal trajectory. This is due to the increase in angle-of-attack at the point of speedbrake failure, which slows the vehicle down at the same time the sink rate is arrested.

The next step in this formulation is to generate sets of neighboring extremals at regular intervals along the trajectory (usually at a one Hz update) and encode neural networks corresponding to these sets. Further, the networks should be modeled such that the level of drag is also an input. This would then mechanize the OPTG method to automatically adapt to speed brake failures. Further extensions of the method will include the other states, velocity and flight path angle, and other critical parameters defining the condition of the vehicle (such as inner-closed-loop bandwidth, as discussed previously).

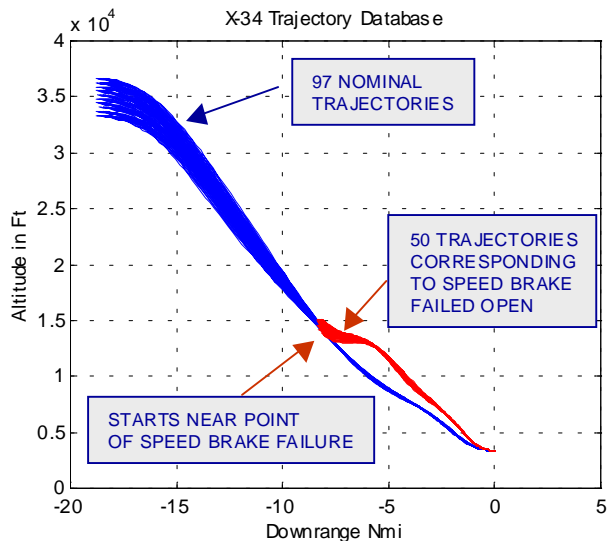


Figure 15. Optimal Trajectory for the Case of Large Drag Deficit.

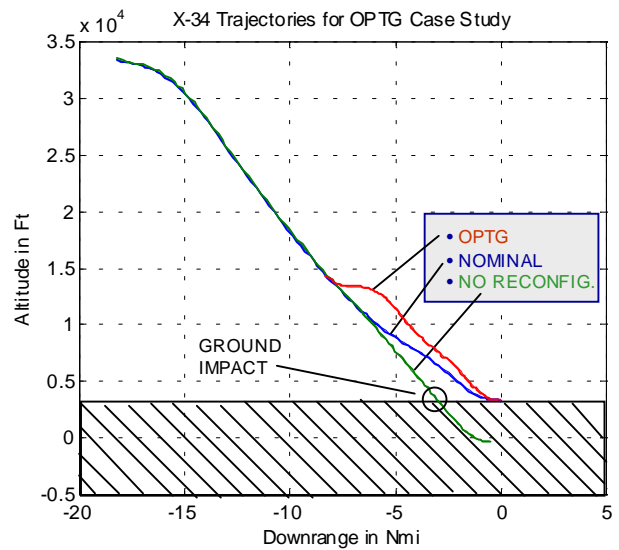


Figure 16. OPTG Trajectory With Speed Brake Failure.

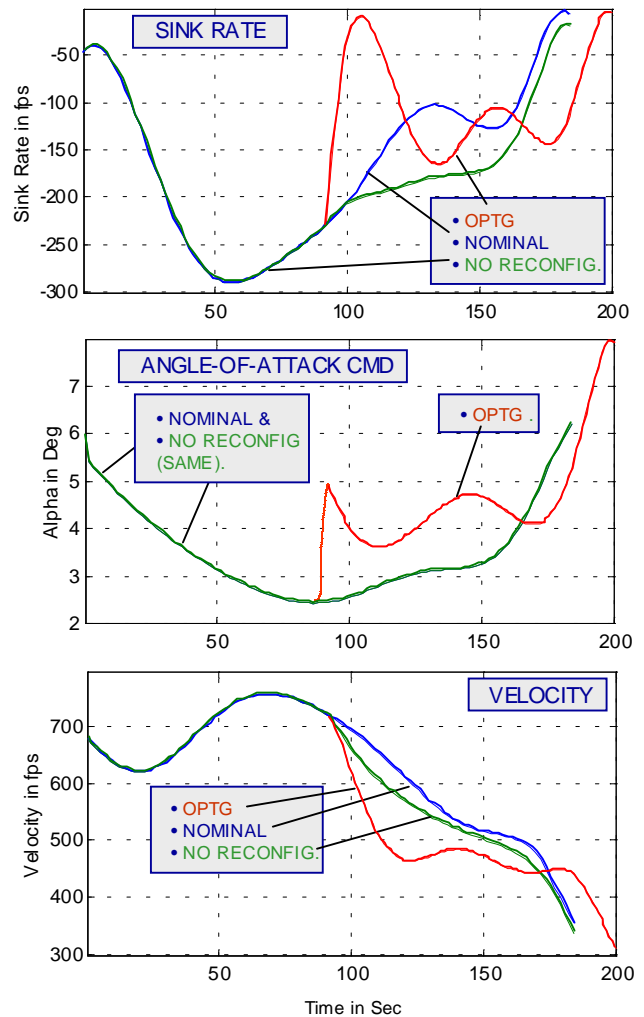


Figure 17. Optimal Trajectory Characteristics.

In addition to the above study, the authors investigated using other optimization strategies to generate trajectory shapes for speed brake failing both closed and wide open. Nonlinear programming (parameter optimization) techniques were investigated, and the formulations considered were to (1) generate continuous angle-of-attack commands, (2) generate angle-of-attack commands at 3-5 discrete switch points and (3) generate flight path angle or flight path angle rate commands at discrete points to yield a small number of fixed curvature flight segments. It is noted that the nonlinear programming formulation provides a more powerful formulation for dealing with inequality constraints, but the COV formulation is ideal for compact trajectory storage per the OPTG algorithm. This work indicated that the formulation which generated a flight path angle rate command results in an equivalent angle of attack command which damps altitude oscillations (Phugoid behavior). This was a problem often seen when directly generating angle of attack commands. Furthermore, by generating flight path angle rate commands, the results to date show well-behaved trajectory generation and numerical stability. Therefore, it is planned to investigate casting the COV formulation in this manner in future OPTG developments.

The results of these additional studies were similar to the results presented above, and it was also noted that speed brake failures are more critical than drag modeling errors. Hence, if optimal trajectories can be found such that the vehicle can successfully land under severe speed brake failures, then landing should be achievable for all drag modeling errors. Furthermore, large headwinds or tailwinds will cause similar effects, and the problem can be generalized to include these effects as well. However, at hypersonic conditions there are greater aerodynamic uncertainties, and the probability of the actual drag being different from the predicted drag is much larger than the probability of speed brake failures. Hence, there is interest in investigating both classes of dynamic changes.

9. CONCLUSIONS

This paper presented a development of an adaptive guidance system for hypersonic RLVs with inner-loop reconfigurable control capabilities. Two main formulations of the proposed guidance system approach were presented.

The Optimal-Path-To-Go/Adaptive Production Guidance (OPTG/APG) system was the first formulation presented. Here, reconfiguration capabilities are integrated into the current production guidance system to provide flight stability following a significant change in the system (such as an effector failure). By utilizing the production guidance system architecture, this approach offers a lower-risk, nearer-term solution to the problem addressed.

A case study developed a preliminary APG system for the approach-to-landing problem under elevon failures. Following an elevon failure, the inner-loop reconfigurable

control system will reallocate pitch control to the *slower* remaining effectors, thereby reducing the inner-closed-loop bandwidth. The change in this critical parameter was rapidly identified by the Modified Sequential Least Squares (MSLS) algorithm and fed to a guidance gain adaptation law. The gains were properly adapted to maintain stability. However, it was shown that re-targeting of the trajectory commands driving the guidance system will typically be required in order to achieve a safe landing. A simplified attempt to re-target the trajectories indicated that the problem is best solved by an on-line automated procedure. It was then proposed to integrate the APG system with the OPTG algorithm to adapt the altitude and altitude rate commands that are fed into the guidance loops.

The OPTG algorithm employs the calculus of variations to design a large database of admissible neighboring extremals. This database is then efficiently expressed in terms of neural network mappings that generate initial values for the co-states. These networks are interrogated on-line at regular intervals, updating the optimal trajectory and the corresponding commands required to follow that trajectory.

A more advanced, longer-term approach was then presented that may offer additional flexibility in the guidance reconfiguration. Here, the OPTG algorithm was used to generate commands that are fed directly into the closed-inner-loop. A proof-of-concept case study was presented where an optimal angle-of-attack command was generated. The OPTG guidance system was able to land the vehicle safely following a mid-course speed-brake failure that added additional drag to the system.

The case studies indicated promising results for both guidance approaches. We recommend that the integrated OPTG/APG approach be further developed to determine the merit of generating optimal commands into the production guidance loops. The advanced OPTG method also requires further development. Preliminary investigations of several alternate formulations have been performed. It is sought to find the best cost function, commands to be generated, and constraints that meet the desired guidance objectives with ease of implementation.

ACKNOWLEDGEMENTS

This work was funded by an Air Force Phase I SBIR program; Dr. David Doman, AFRL/VACA, Program Manager. *Their support is gratefully appreciated.*

REFERENCES

- [1] Pamadi, B., Brauckmann, G., Ruth, M., "Aerodynamic Characteristics, Database Development and Flight Simulation of the X-34 Vehicle," AIAA Paper No. 2000-0900, *Proceedings, 38th Aerospace Sciences Meeting & Exhibit*, Reno, NV, 2000.

[2] Lindberg, R., and R. Feconda, "The X-34: Versatile RLV Technology Test Bed," *Aerospace America*, Aug. 1998.

[3] Ward, D., J. Monaco, and M. Bodson, "Development and flight testing of a parameter identification algorithm for reconfigurable control," *Journal of Guidance, Control, and Dynamics*, Vol. 21, No. 6, Nov. – Dec. 1998, pp. 948-956.

[4] Corban, J., Calise, A., Flandro, G., "Rapid Near-Optimal Aerospace Plane Trajectory Generation and Guidance," *Journal of Guidance, Control, and Dynamics*, Vol. 14, No. 6, 1991, pp. 1181-1190.

[5] Chavez, F., Schmidt, D., "Analytic Aeropropulsive/Aeroelastic Hypersonic-Vehicle Model with Dynamic Analysis," *Journal of Guidance, Control, and Dynamics*, Vol. 17, No. 6, 1994, pp. 1308-1319.

[6] Schmidt, D., "Optimum Mission Performance and Multivariable Flight Guidance for Airbreathing Launch Vehicles," *Journal of Guidance, Control, and Dynamics*, Vol. 20, No. 6, 1997.

[7] Schmidt, D., Lovell, T., "Mission Performance and Design Sensitivities for Hypersonic Airbreathing Vehicles," *Journal of Spacecraft and Rockets*, Vol. 34, No. 2, 1997, pp. 158-164.

[8] Schmidt, D., Hermann, J., "Use of Energy-State Analysis on a Generic Air-Breathing Hypersonic Vehicle," *Journal of Guidance, Control, and Dynamics*, Vol. 21, No. 1, 1998, pp. 71-76.

[9] Lu, P., "Regulation About Time-Varying Trajectories: Precision Entry Guidance Illustrated," *Journal of Guidance, Control, and Dynamics*, Vol. 22, No. 6, 1999, pp. 784-790.

[10] Mease, K., *et. al*, "Re-Entry Trajectory Planning for a Reusable Launch Vehicle," AIAA Paper No. 99-4160, *Proceedings: AIAA Guidance, Navigation, and Control Conf.*, Portland, OR, Aug. 1999.

[11] Ward, D., Monaco, J., Schierman, J., "Reconfigurable control for VTOL UAV shipboard landing," AIAA Paper No. 99-4045, *Proceedings: AIAA Guidance, Navigation, and Control Conf.*, Portland, OR, Aug. 1999.

[12] Bateman, A., D. Ward, R. Barron, J. Monaco, J. Hull, Hydra-7 Guidance Law Development, Barron Associates, Inc. Final Technical Report for Lockheed Martin Advanced Projects, Contract N00174-98-C-0030, Nov. 1999.

[13] Kirk, D., *Optimal Control Theory, An Introduction*, Prentice-Hall Electrical Engineering Series, Englewood Cliffs, New Jersey, 1970.

[14] Pierre, D., *Optimization Theory with Applications*, Dover Publications, Inc., New York, 1986.



John Schierman obtained his Ph.D. from Arizona State University in 1996, his Master's from Purdue University in 1988, and his Bachelor's degree from Georgia Tech in 1984, all in Aerospace Engineering. He worked as a faculty research associate at the University of Maryland and as a systems engineer for Boeing Aircraft and Missile Systems. Dr. Schierman joined Barron Associates, Inc. in 1999. His current research interests include adaptive/reconfigurable, nonlinear control and guidance systems. Dr. Schierman is a member of AIAA, ASME, the American Society of Naval Engineers (ASNE), and the American Society for Engineering Education (ASEE).

David Ward received a Bachelor's degree in Electrical Engineering in 1985, and a Master's degree in Computer and Systems Engineering in 1986 from Rensselaer Polytechnic Institute. Mr. Ward joined Barron Associates, Inc. in 1991, and his current research interests include neural networks, parameter identification, and robust adaptive nonlinear flight control. Mr. Ward is a member of the IEEE, AIAA, and the Society for Industrial and Applied Mathematics (SIAM). He has a number of U.S. patent applications pending.

Jason Hull received his B.S. degree in Electrical Engineering from Rensselaer Polytechnic Institute in 1997. Prior to joining BAI in 1999, Mr. Hull worked as an Electrical Design Engineer at GE Fanuc. His current research interests include optimization techniques for guidance law development, parameter identification and neural networks.

Jeff Monaco received the B.S. degree in Engineering Science and Mechanics with a minor in Mathematics in 1992, and the M.S. degree in Engineering Mechanics in 1994 all from Virginia Tech. He joined Barron Associates, Inc. in 1994, and his current research interests include adaptive control techniques, reconfigurable primary flight control applications, development of optimal guidance and limit-avoidance systems. Mr. Monaco is a member of IEEE and AIAA and has several U.S. patent applications pending.

Mike Ruth received his Bachelor's of Science degree in Mechanical Engineering from Duke University in 1982, and his Master's of Science in Applied Mechanics from the California Institute of Technology in 1983. Mr. Ruth joined Orbital Science Corporation's Dulles, VA office in 1996, and is currently the manager of the Guidance, Navigation and Control, Advanced Programs Group. He has also worked for Vehicle Control Technologies, Inc., ARAP Group, California Research and Technology, Inc., and Johns Hopkins University Applied Physics Lab. Mr. Ruth is a member of AIAA and the Institute of Navigation.